2007-01-0465

Newly Developed Functionalities for the Virtual Human Santos

Jingzhou Yang, Xiaolin Man, Yujiang Xiang, Hyun-Joo Kim, Amos Patrick, Colby Swan, Karim Abdel-Malek, and Jasbir Arora
Center for Computer-Aided, The University of Iowa, Iowa City, IA 52246

ABSTRACT

This paper presents newly developed capabilities for the virtual human Santos™. Santos is an avatar that has extensive modeling and simulation features. It is a digital human with 109 degrees of freedom (DOF), an optimization-based method, predictive dynamics, and realistic human appearance. The new capabilities include (1) significant progress in predictive dynamics (walking and running), (2) advanced clothing modeling and simulation, (3) muscle wrapping and sliding, and (4) hand biomechanics. With these newly developed functionalities, Santos can simulate various dynamic tasks such as walking and running, investigate clothing restrictions to motion such as joint limits and torques, simulate the musculoskeletal system in real time, predict hand injury by monitoring the joint torques, and facilitate vehicle interior design. Finally, additional on-going projects are summarized.

Keywords: Virtual humans, predictive dynamics, muscle wrapping, hand biomechanics.

INTRODUCTION

Virtual human modeling and simulation has gained significant momentum in recent years. High-performance computers make it possible, and the game, movie, and medical industries accelerate it. Product design is another important field for virtual humans. Virtual humans make it possible to reduce design costs and cycle time and increase quality and safety.

Several commercial software programs are available, including Jack®, RAMSIS®, and Safework®. However, none of them has the complete functionality required to meet our needs—predicted posture, predictive dynamics, realistic human appearance, etc. To satisfy this need, the US Army launched a research effort several years ago to develop Santos. Santos has a physical-based environment (Yang et al., 2004; Yang et al., 2005; Yang et al., 2006a; Yang et al., 2006b; Abdel-malek et al., 2006) and a human-like appearance. Because it is a musculoskeletal human model, it can answer different types of questions (e.g., whether Santos has enough energy to walk from Point A to Point B and, if so, what the discomfort level will be).

In previous reports, we have proposed different capabilities such as optimization-based posture prediction, advanced posture prediction, dynamic motion prediction, advanced inverse kinematics, muscle stress analysis, a hand model, and physiological analysis. In this paper, we present newly developed capabilities, including predictive dynamics, advanced clothing modeling, muscle wrapping and sliding, and hand biomechanics.

PREDICTIVE DYNAMICS

Traditionally, there are forward and inverse dynamics. In forward dynamics, we try to find the kinematic properties given the external forces; in inverse dynamics, we try to find the external forces given the motion. However, in predictive dynamics, we predict the motion without being given the complete set of external forces and motion. We use an optimization technique to solve this problem. The formulation is illustrated as follows:

Find: Joint angle profiles $\mathbf{q}$
to minimize: Human performance measures
subject to: Constraints

For different tasks, the detailed terms in this formulation will vary. In this section, we present the progress in two specific tasks: walking and running.

SIMULATION OF HUMAN WALKING

The task of walking from point A to point B is divided into three stages, as depicted in Figure 1. The initial stage starts from a standing-still position and goes to the end of the initial stride; it includes two steps, one with initial

step length and the other with normal step length. The normal stage starts at the final posture of the initial stage and continues to a normal stride with two normal step lengths; the ending posture is the same as the starting posture in the normal stage, so the normal stride can be repeated as shown in Figure 2. The final stage begins with the final posture of the normal stage and continues to the required stopping condition.

The joint angle profiles are determined for each stage. Once each stage has been solved, more general walking problems can be dealt with by repeating the normal stage to cover the desired distance, as shown in Figure 2.

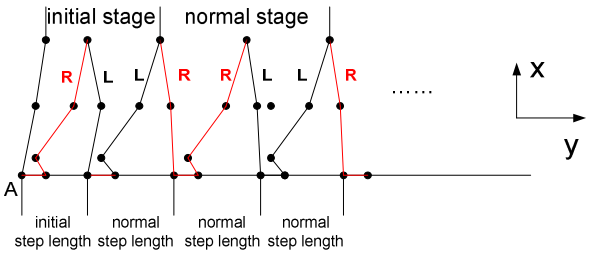

Figure 1 Three stages of walking from Point A to Point B (L is left leg, R is right leg)

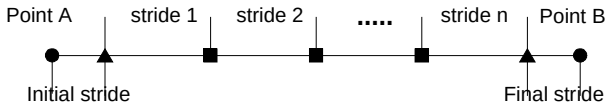

Figure 2 Long-distance walking

The optimization formulation is defined as follows:

Design variable: Joint angle profiles $\mathbf{q}$

Cost function: Minimize the maximum torque

$$Min\ f(q,\dot{q},\ddot{q}) = Max(\tau_i(t)) \qquad i = 1...ndof, \quad 0 < t < T \tag{1}$$

where $\tau_i = tr[\ \frac{\partial \mathbf{A}_i}{\partial q_i}\mathbf{D}_i\ ] - \mathbf{g}^{\mathrm{T}}\frac{\partial \mathbf{A}_i}{\partial q_i}\mathbf{E}_i$, $\mathbf{D}_i = \mathbf{J}_i\mathbf{C}_i^{\mathrm{T}} + \mathbf{T}_{i+1}\mathbf{D}_{i+1}$,

$\mathbf{E}_i = m_i\,{}^i\mathbf{r}_i + \mathbf{T}_{i+1}\mathbf{E}_{i+1}$, $\mathbf{A}_j = \mathbf{T}_1\ \mathbf{T}_2\ \mathbf{T}_3\cdots\mathbf{T}_j = \mathbf{A}_{j\text{-}1}\mathbf{T}_j$,

$\mathbf{B}_j = \dot{\mathbf{A}}_j = \mathbf{B}_{j\text{-}1}\mathbf{T}_j + \mathbf{A}_{j\text{-}1}\frac{\partial \mathbf{T}_j}{\partial q_j}\dot{q}_j$,

$\mathbf{C}_j = \dot{\mathbf{B}}_j = \ddot{\mathbf{A}}_j = \mathbf{C}_{j\text{-}1}\mathbf{T}_j + 2\mathbf{B}_{j\text{-}1}\frac{\partial \mathbf{T}_j}{\partial q_j}\dot{q}_j + \mathbf{A}_{j\text{-}1}\frac{\partial^2 \mathbf{T}_j}{\partial q_j^{\,2}}\dot{q}_j^{\,2} + \mathbf{A}_{j\text{-}1}\frac{\partial \mathbf{T}_j}{\partial q_j}\ddot{q}_j$

, $\mathbf{T}_j$ is the transformation matrix, $\mathbf{D}_{n+1} = \mathbf{E}_{n+1} = [\ \mathbf{0}\ ]$, $\mathbf{J}_i$ is inertia matrix for link i, m_i is mass of link i, $\mathbf{g}$ is the gravity vector, ${}^i\mathbf{r}_i$ is the location of the center of mass of link i in link i frame, $tr[\ \cdots]$ denotes the trace operation, and $(\cdots)^{\mathrm{T}}$ denotes the matrix transpose.

Constraint 1: Joint angle limits

$$\mathbf{q}^L \le \mathbf{q} \le \mathbf{q}^U, \qquad 0 \le t \le T \tag{2}$$

Constraint 2: Foot ground penetration in each phase (controls height of foot points as shown in Figure 3):
(1) Foot point without contact (triangular points in Figure 3):

$$x_i \ge 0, \qquad 0 \le t \le T_{phase(j)} \tag{3}$$

(2) Foot point with contact condition (circular points in Figure 3):

$$x_i = 0 \quad , \quad 0 \le t \le T_{phase(j)} \tag{4}$$

where i is foot point index and j is the phase index

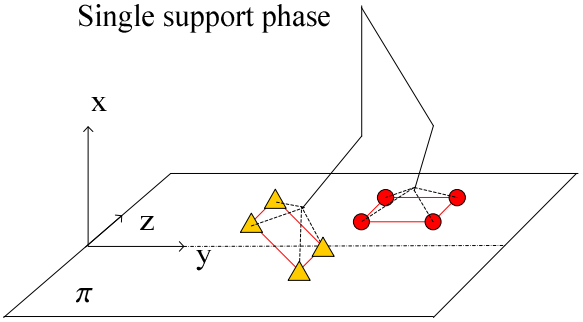

Figure 3 Foot Points Penetration Constraints

Constraint 3: Foot strike position (this condition can determine walking direction and step length):

$y_i(t) = y_s$, (rectangular points in Figure 4)

$z_i(t) = z_s$, t = initial, final, and heel strike (5)

where i is the foot point index and s is the specified contacting point position

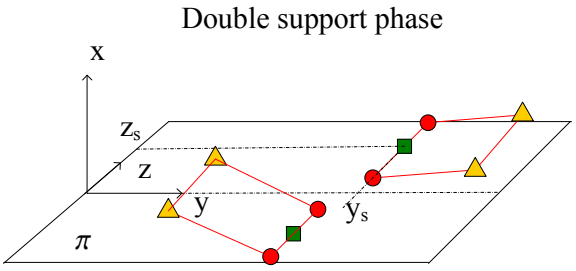

Figure 4 Foot strike position constraints

Constraint 4: Zero moment point (ZMP) stability:

$$y_{ZMP} = \frac{\sum_{i=1}^{ndof} m_i(\ddot{x}_i + g)y_i - m_i\ddot{y}_i x_i + I_i\ddot{\theta}_{iz}}{\sum_{i=1}^{ndof} m_i(\ddot{x}_i + g)} \in FSR$$

$$z_{ZMP} = \frac{\sum_{i=1}^{ndof} m_i(\ddot{x}_i + g)z_i - m_i\ddot{z}_i x_i + I_i\ddot{\theta}_{iy}}{\sum_{i=1}^{ndof} m_i(\ddot{x}_i + g)} \in FSR \qquad (6)$$

where x_i, y_i, and z_i are the coordinates of the center of mass for i^{th} link, and *FSR* is the foot support region. m_i is the mass of the i^{th} link, I_i is the global inertia of the i^{th} link, and $\ddot{\theta}_i$ is the global angular acceleration of the i^{th} link.

Constraint 5: Continuity condition: starting posture $\mathbf{q_0}$ of the normal stage is the same as ending posture $\mathbf{q}_{Tinitial}$ of the initial stage, and final posture of the normal stage $\mathbf{q}_{Tnormal}$ is the same as the starting posture of the normal stage, except for the global translational DOF along the gait axis.

$$\mathbf{q_0} = \mathbf{q}_{T_{initial}}$$
$$\mathbf{q_0} = \mathbf{q}_{T_{normal}} \notin \textit{global translational DOF} \qquad (7)$$

where $T_{initial}$ is the final time of initial stage and T_{normal} is the final time of normal stage.

The initial and normal stages were optimized using the formulations described above. The final stage is dependent on the total distance of the walking task. The results shown here are for one initial stage and three repeated normal stages with 18 DOFs in the lower body. The overall progression of motion, joint angles, velocity, and acceleration profiles for the right leg are shown in Figure 5.

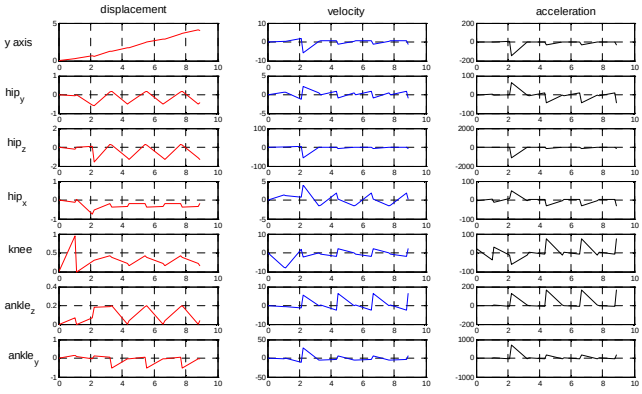

Figure 5 Progression and right leg joint motion

Joint torque profiles can be obtained from the optimal solution. The torque profiles for the right leg are shown in Figure 6. Note that since the ground reaction forces are not considered in the current formulation, the torques are only due to gravity, inertia, and Coriolis effect.

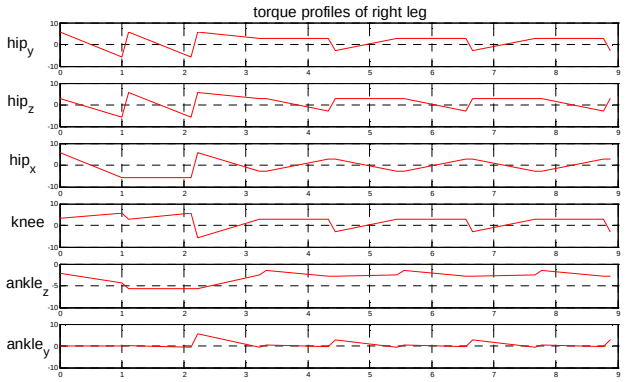

Figure 6 Torque profiles of right leg

The motion in the saggital plan is shown in Figure 7, including one initial stage and three normal stages.

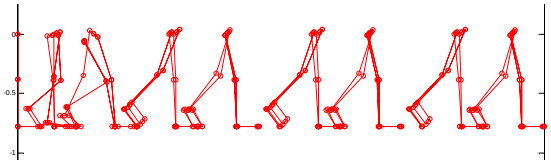

Figure 7 Saggital plan motion

SIMULATION OF HUMAN RUNNING

The running style depends on the speed of running. For example, at slower running speeds, the heel touches the ground first. In fast running or sprinting, the fore-foot touches the ground first. Moreover, the upper body motion is different for the slower and faster running (sprint) cases. The faster the speed, the more arm swinging motion is generated to minimize energy consumption. Running is differentiated from walking not by the speed but by the existence of a flight phase. During a walk, whether slow or fast, there exists a double support phase (where both feet are on the ground).

The period from the initial contact of one foot to the following contact of the same foot is called the *gait cycle*. One gait cycle of running is composed of two phases: the support phase and the flight phase. The flight phase starts with a toe-off and ends with the strike of the other foot. The support phase starts with a foot strike and ends with same foot's toe-off (Figure 8). In the area of biomechanics, the length from one foot's strike to the other foot's strike is called a *step*. Also, the length from one foot's strike to the same foot's subsequent strike is called a *stride*.

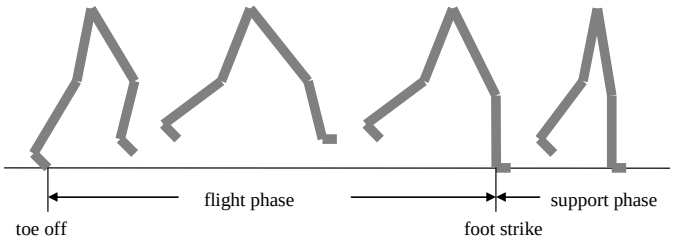

Figure 8 Human running cycle

The formulation for the task of human running is defined as follows:

Design Variables: **q**, **τ**, **F**
where **q** is joint angle profiles, **τ** is joint torque profiles, and **F** is foot contact force profile.

Cost function:

$$f = \int_0^{t1} \tau_s^T \tau_s dt + I_{toff}^T I_{toff} + \int_{t1}^{t} \tau_f^T \tau_f dt + I_{strk}^T I_{strk} \quad (8)$$

where I_{toff} is toe-off phase impulse, I_{strk} is foot strike phase impulse, and τ_s is the joint torque for joint *s*.

Constraints:

- Foot location of heel contact point
- Ground penetration
- ZMP
- Joint limits/torque limits
- Equations of motion
- Conservation of angular momentum

The simulation example shown in Figure 9 is the result of a lower body with 18 DOF in the Santos environment.

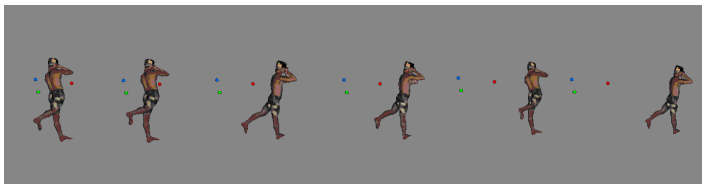

Figure 9 Snapshot of Santos running

CLOTHING MODELING AND SIMULATION

Since the current work is aimed at accurate and physically realistic modeling of clothing interactions with the human body, the continuum surface approach is adopted for modeling clothing in this effort (Man et al., 2006). This framework is both mathematically and mechanically rigorous and provides a clear relationship between fabric stress-strain relations and the forces/displacements in the discretized model.

The human model is grossly represented by an assemblage of rigid ellipsoids, and the kinematics data of human motion are collected using motion capture to record the motion of each ellipsoidal segment. As each ellipsoid is treated as a rigid entity, the space it occupies at any instant in time is determined by the location of the centroid and the orientation of the ellipsoid.

Based on the proposed computational framework, the mechanical interactions between clothing and a wearer can be quantified. A general procedure is as follows: Given the wearer's motions, the contact tractions between clothing and human body surfaces are solved and the stresses and the strains in clothing fabrics are determined as well. These mechanical quantities are then related to certain predefined restriction measures, such as joint torque or energy expenditure, to quantify the effect of clothing on the wearer for the given motion. Currently the motion is prescribed and is assumed to be independent of the clothing restrictions. Two examples will be provided; the first illustrates arm-sleeve interaction, and the second illustrates the interaction of pants with walking/stepping legs.

ARM-SLEEVE INTERACTION STUDY

The motion considered is flexing the forearm about the elbow joint while keeping the upper arm fixed. The torque exerted by the sleeve about the elbow joint is calculated. The sleeve is modeled as a cylindrical tube with length L = 0.5 m, radius R = 0.06 m, and thickness t = 1 mm. Boundary conditions are specified to restrain the motion of fabric nodes around the shoulder. The upper arms and forearms are modeled as two ellipsoids, one fixed in space and the other rotating about the joint with a constant angular velocity. The total rotation angle is 57° before severe clothing self-contact occurs. The material properties used in the computation are as follows: Young's modulus in the warp and weft directions E = 1.2 MPa, shear modulus G = 0.1 MPa, and mass density ρ = 436 kg/m^3.

The friction between clothing and human body surface is an important factor affecting the interaction of the two. For a sleeve model with a well-refined mesh, the low-friction case ($\mu = 0.1$) is compared with a high-friction case ($\mu = 0.5$). It is found that in the low friction case the sleeve slips down as the forearm rotates upward. Alternatively, in the high-friction case, the sleeve does not slide down the forearm. Snapshots of the sleeve deformation for both the low- and high-friction cases are shown in Figure 10 at two elbow flexion angles, $\alpha = 37^\circ$ and $\alpha = 57^\circ$.

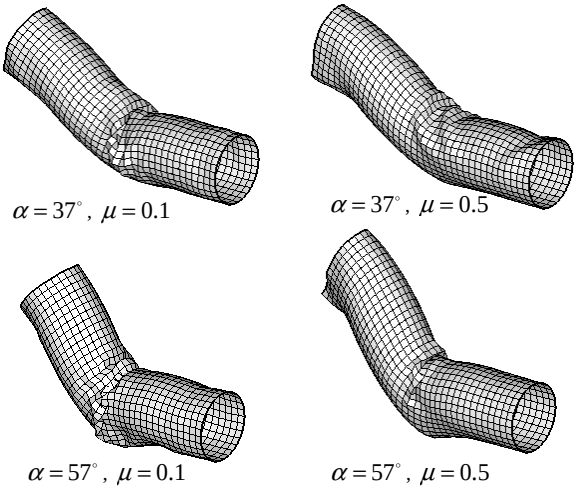

Figure 10 Sleeve deformation for different friction coefficients

To briefly study the effect of clothing fit on resistance, the radius of the sleeve tube is increased to R = 0.07 m from R = 0.06 m, while the dimensions of the ellipsoidal arms remain the same. The resisting torque exerted by the looser-fitting sleeve (Figure 11a) is compared with that of the original tighter-fitting sleeve (Figure 11b). For both fits, a skin surface friction coefficient $\mu = 0.5$ is used. The computed resisting torque exerted by the looser-fitting sleeve (Figure 12) is significantly less than that of the tighter-fitting sleeve for elbow flexion angles greater than 20°.

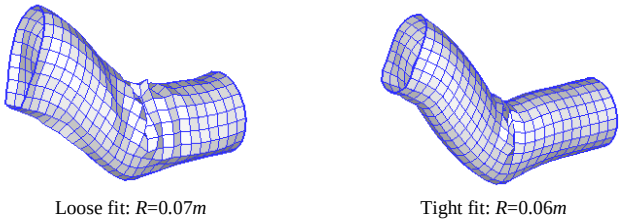

Figure 11 Deformed configurations of sleeves with different radii

Fabric thickness is another factor that can affect clothing-wearer interaction. A thicker fabric has greater mass and larger stiffnesses. Membrane stiffnesses increase in proportion to the fabric thickness, while the bending stiffnesses increase in proportion to the thickness cubed. Here, the thickness of the sleeve fabric is doubled to t = 2 mm, and the joint torque is compared with the original case where t = 1 mm. All other properties remain the same, and a surface friction coefficient μ = 0.5 is assumed. The computed torque resistance of the thicker fabric is roughly double that of the thinner fabric, which indicates that membrane rather than bending behavior of the sleeve is dominant (see Figure 13).

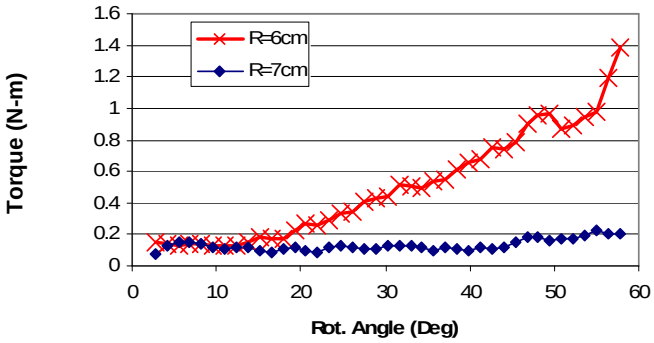

Figure 12 Computed resisting torques exerted by sleeves with different radii

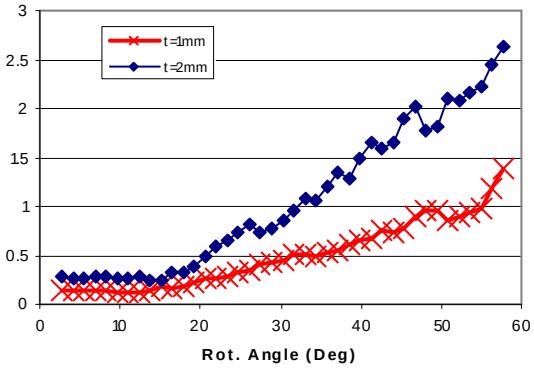

Figure 13 Comparison of sleeve torque resistance with different fabric thickness

INTERACTION OF PANTS WITH WALKING/STEPPING LEGS

In this problem, a human subject walked four strides, with the third involving stepping over an obstacle 0.5 m in height. The motion of this human was captured with an array of eight infrared VICON cameras, and the motions were then mapped onto the assemblage of ellipsoids to make them walk. A pair of pants was then placed onto the human model (see Figure 14) in the following sequence: (a) the feet of the human model were removed; (b) the pants were pulled up over the legs and pelvis of the human model; (c) the feet of the human model were restored; and (d) the effect of a belt was created by tensioning the fabric at the waistline. With the garment on the human model, a simulation of the interaction between the pants and the lower body walking and crossing the obstacle was then undertaken (see Figure 15). Two sets of pants were modeled, both made of compliant, crimped cotton. The first pair had a

thickness of 1 mm, and the second had a thickness of 2 mm. The resistance torques are shown in Figure 16.

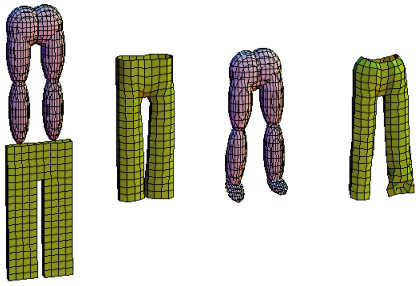

Figure 14 Sequence for the human model to don a pair of pants

Figure 15 Simulation of pants interacting with lower body striding and then stepping over an obstacle

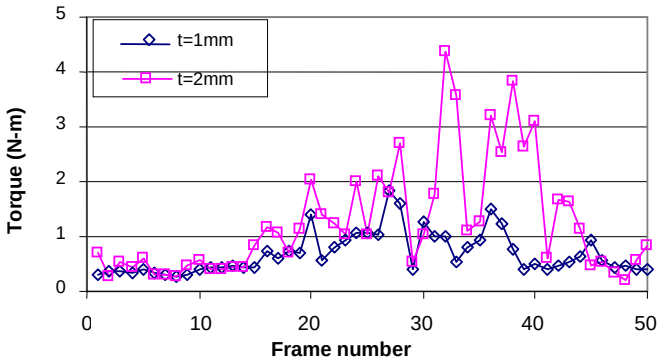

Figure 16 Computed resistance torques exerted by two pairs of cotton pants of different fabric thicknesses about the right knee

MAIN SECTIONDYNAMIC MUSCLE WRAPPING AND SLIDING

In this section, we present a method for real-time approximation of how muscles wrap around underlying structures. This was accomplished by allowing floating via points to dynamically wrap around prescribed obstacles and implementing this in the Santos environment.

Wrapping algorithms use prescribed obstacles to bend the action line of a muscle in real time so that the action line is a reasonable approximation of the real muscle's action line for all possible joint configurations. From anatomy, we can determine the origin and insertion of a particular muscle. We can also analyze underlying muscles and bones to determine the size, shape, position, and number of obstacles that the muscle being modeled must wrap around. Therefore, the unknowns are the positions of the intermediate floating via points. These positions are dependent upon two factors: whether there are one or more obstacles about which wrapping should occur and, if so, the shape and position of the obstacle or obstacles.

An action line will be used to idealize the direction of force generated by a single muscle. The model attempts to use obstacles to push the line so that it approximates the centroid line of the muscle, regardless of the orientation of the arm. Some muscles with wide attachment points or multiple heads such as the biceps use multiple action lines. All action lines consist of an origin point at one end, an insertion point at the other end, and a number of floating via points in between. Each point is connected to the next with a straight line (Figure 17). Obstacles consist of a simple sphere or cylinder; therefore, wrapping algorithms are developed for each obstacle. The detailed algorithms were reported by Patrick (2005).

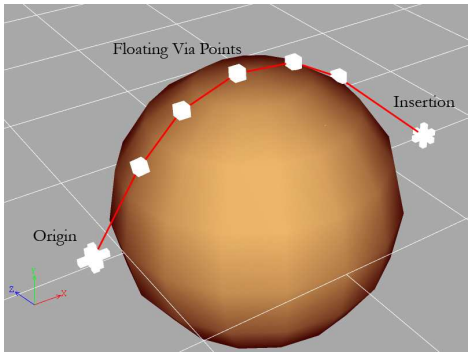

Figure 17 Example of wrapping about a sphere

When attaching the muscles to the kinematic model, two factors are of great importance. The first is the shape of the muscle and where it originates and inserts on the skeleton. Since the muscles are working in bones that are arranged in a lever-like structure, determining the correct attachment points is critical because there is a direct correlation between these and the torque the associated muscle can create. This is addressed by using an accurate geometric model of the musculoskeletal system to locate the origin and insertion points. Furthermore, the shape of the muscle is critical in determining the direction of the force created by the muscle. For example, as the elbow is flexed, the direction of the force on the radius created by the biceps is related to the angle of pronation of the hand because the biceps may wrap around the radius, the angle of the

flexion of the elbow because the biceps may need to wrap over the distal end if the humerus or the brachialis, and the orientation of the humerus because both heads actually attach to the scapula (see Figure 18). This is addressed by incorporating real-time wrapping algorithms and wrapping obstacles that affect the action line of the muscle, creating an approximation of the centroid line of the muscles that change with the orientation of the limb. The development and application of these algorithms was covered in the previous section.

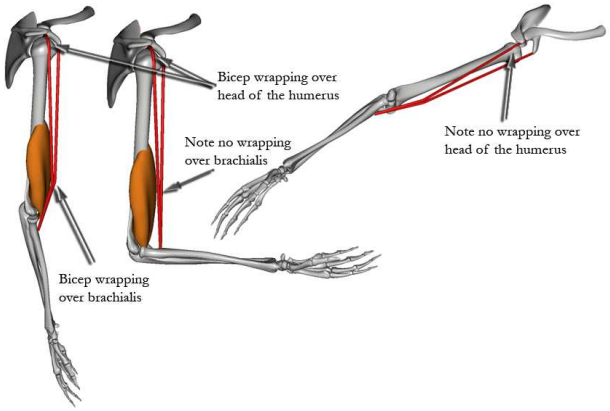

Figure 18 Effects of muscle wrapping as applied to the biceps

The second factor that is significant when attaching the muscles to the skeletal model is the number of action lines used to approximate the force generated by a muscle. For computational reasons, the muscles will need to be idealized as a number of action lines along which the tension being created by the muscle will act. Obviously, the more action lines one models, the more accurate the model will become. However, for the model to be useful and to fulfill the requirement of being real-time, a balance between computational expense and accuracy must be found. For many muscles, such as the biceps, a single action line is adequate because the origin and insertion points are small. For other muscles, such as the trapezius, the insertion and/or origin cover a wide area, so a single action line is not an appropriate approximation (see Figure 19). Van der Helm and Veenbaas (1991) compared the moment vector calculated from a large number of action lines (200) and compared it to the moment vector calculated from a reduced number (6) and found the error to be minimal. Therefore an appropriate model should include six action lines for several muscles in the shoulder. Our model, however, will be developed in a manner similar to the model presented by Maurel and Thalmann (1999) in which the number of action lines will be less. Once this model is finished, the real-time performance will be evaluated, and more action lines will be considered.

With the above factors considered, the muscles of the limbs were modeled as shown in Figure 20. This resulted in 134 action lines, each with one or more wrapping obstacles. Furthermore, the bones were jointed into an appropriate kinematic skeleton and interaction was added so that the user had the ability to manipulate any of the joints. The result was a skeleton with real-time interaction as well as live muscle wrapping and sliding, all running at 30+ fps.

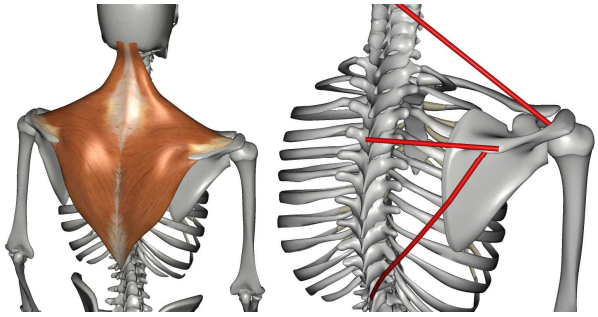

Figure 19 The trapezius and its action lines

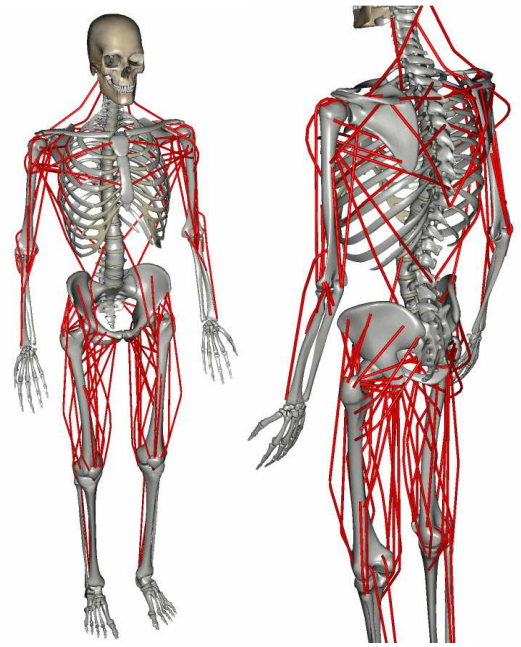

Figure 20 Current modeled action lines

HAND BIOMECHANICS

In the previous report (Pena Pitarch et al., 2005), we developed the 25-DOF hand model, and in this section we will present the hand biomechanics. There are two parts: (1) given finger contact forces, we want to find the joint torques; (2) given joint torques, we want to determine the finger contact forces.

A hand musculoskeletal and grasping model is shown in Figure 21. The assumption for grasping is that the contact point is at the middle point of each link. $\boldsymbol{\tau}^j$ represents the joint torque vectors for finger j, where

$j = 1, \cdots, 5$, $\boldsymbol{\tau}^j = [\tau_1^j, \tau_2^j, ..., \tau_{ni}^j]^T$, n_i denotes the total degrees of freedom for finger j, and $\mathbf{F}_i^j$ represents the contact forces between the object and link i for finger j.

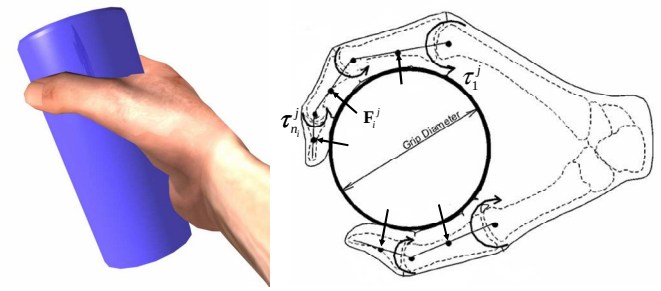

(a) Grasp an object (b) Contact forces and joint torques
Figure 21 Grasping model

Since the hand grasping velocity and acceleration are small, we consider hand grasping as one static problem. Therefore, finger joint torques will be the general static torques. The relationship between the joint torque vector and end-effector force/moment vector for finger j is then given by

$$\boldsymbol{\tau}^j = \mathbf{J}^T \mathbf{F}^j \tag{9}$$

Now we extend this formulation to the case where multiple external loads (both translational and rotational) are applied to any location of any finger/link, not necessarily to the end-effector. Let's assume that a general form of external load $\mathbf{F}_k^j$ is applied to the point at $\mathbf{k}_{r_k}$ location of finger segment k, where $\mathbf{k}_{r_k}$ location vector is expressed with respect to the k^{th} local coordinate frame.

This point of application of external load can be regarded as the end-effector for the corresponding external load. So the joint torque vector due to the external load applied at point $\mathbf{k}_{r_k}$ of link *k* is

$$\boldsymbol{\tau}_k^j = \mathbf{J}_k^T \mathbf{F}_k^j \tag{10}$$

where $\mathbf{J}_k$ is the augmented Jacobian matrix for this point. From the principle of superposition, the total joint torques due to several external loads are obtained as a sum of all joint torques, as follows:

$$\boldsymbol{\tau}^j = \sum_k \mathbf{J}_k^T \mathbf{F}_k^j \tag{11}$$

One example of this problem is that the right hand grasps one object and the contact forces are 2 Newtons at each contact point of the finger segments. The joint torques are shown in Figure 22.

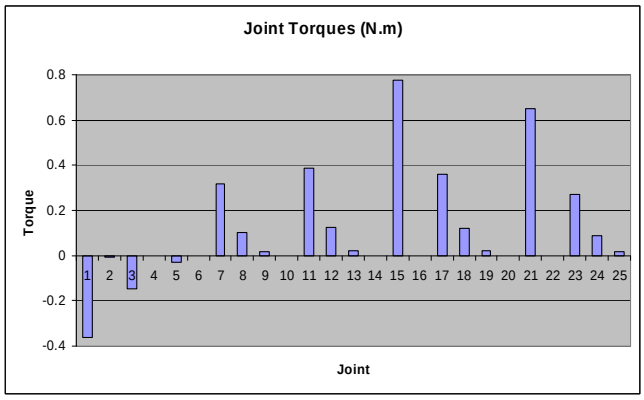

Figure 22 Finger joint torque

Another problem is that given the joint torques we try to find the finger contact forces. Figure 23 shows the free body diagram of one finger. Based on Eq. (11), if $\mathbf{F}_{n_i}^j$ is applied on link n_i, the joint torque for joint n_i will be defined by

$$\tau_{n_i}^j = (J_{n_i-1}^{n_i})^T F_{n_i}^j \tag{12}$$

For link $n_i - 1$, we have the following equation:

$$\tau_{n_i-1}^j = (J_{n_i-1}^{n_i})^T F_{n_i}^j + (J_{n_i-2}^{n_i-1})^T F_{n_i-1}^j \tag{13}$$

Similarly, for other links and joints we have

$$\begin{aligned} &\vdots \\ \tau_1^j &= (J_{n_i-1}^{n_i})^T F_{n_i}^j + (J_{n_i-2}^{n_i-1})^T F_{n_i-1}^j + \cdots + (J_0^1)^T F_1^j \end{aligned} \tag{14}$$

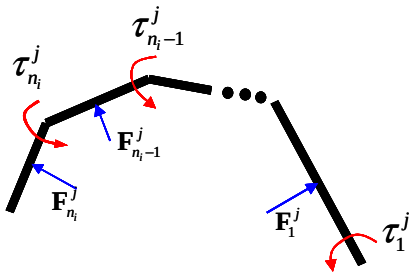

Figure 23 Joint torques and the contact forces diagram

From Eq. (12) we get

$$F_{n_i}^j = (J_{n_i-1}^{n_i})^{-T} \tau_{n_i}^j \tag{15}$$

Plugging in Eq. (15) to Eq. (13) and we obtain

$$F_{n_i-1}^j = (J_{n_i-2}^{n_i-1})^{-T} (\tau_{n_i-1}^j - \tau_{n_i}^j) \tag{16}$$

Similarly, we can derive contact forces for other links. Suppose the given joint torques are shown in Figure 24. We use the proposed method, and the calculated finger contact forces are 3.5 N, 4.0 N, 2.5 N, 3.0 N, and 2.5 N for the thumb, index, middle, ring, and pinky fingers, respectively.

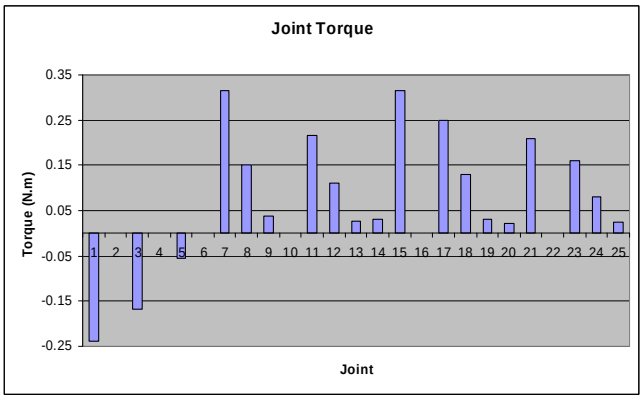

Figure 24 Given joint torques

SUMMARY AND CONCLUSION

The following newly developed functionalities for Santos have been demonstrated: predictive dynamics, which includes the simulation of human walking and running; clothing modeling and simulation; detailed muscle wrapping and sliding; and hand biomechanics, which is a necessary step for grasping simulation and a useful tool for predicting hand injury. Several projects are ongoing: predictive dynamics, which will include other tasks such as whole-body swinging, diving, and jumping; grasping, which involves Santos grasping different objects and providing feedback about the grasp quality; and advanced clothing modeling. The ultimate goal is for the Santos model to do many different tasks on its own. In the meantime, the environment provides feedback in areas such as discomfort level and energy consumption.

ACKNOWLEDGES

This research is funded partly by the US Army TACOM project “Digital Humans and Virtual Reality for Future Combat Systems (FCS) (DAAE07-03-D-L003)”, the Caterpillar Inc. project “Digital Human Modeling for Safety and Serviceability,” and the US Army Natick National Soldier Research Center project “Biomechanical Simulator System (BAS).”

REFERENCES

Abdel-Malek, K., Yang, J., Marler, T., Beck, S., Mathai, A., Patrick, A., and Arora, J., (2006), “Towards a New Generation of Virtual Humans,” *International Journal of Human Factors Modelling and Simulation*, Vol. 1, No. 1, pp. 2-39.

Kim, J., Abdel-Malek, K., Yang, J., and Marler, T., (2006), “Prediction and Analysis of Human Motion Dynamics Performing Various Tasks,” *International Journal of Human Factors Modelling and Simulation*, Vol. 1, No. 1, pp. 69-94.

Maurel, W. and Thalmann, D. (1999), “A case study on human upper limb modeling for dynamic simulations,” *Computer Methods in Biomechanics and Biomedical Engineering*, Vol. 2, No. 1, pp. 65-82.

Man, X., Swan, C., and Rahmatalla, S. (2006), “A Clothing Modeling Framework for Uniform and Armor System Design,” Modeling and Simulation for Military Applications. *Proceedings of the SPIE*, Vol. 6228.

Maurel, W. and Thalmann, D. (1999), “A case study on human upper limb modeling for dynamic simulations,” *Computer Methods in Biomechanics and Biomedical Engineering*, Vol. 2, No. 1, pp. 65-82.

Maurel, W. and Thalmann, D. (1999), “A case study on human upper limb modeling for dynamic simulations”, *Computer Methods in Biomechanics and Biomedical Engineering*, Vol. 2, No. 1, pp. 65-82.

Patrick, A. (2005), “Development of a 3D Model of the Human Arm for Real-Time Interaction and Muscle Activation Prediction,” MS Thesis, The University of Iowa, December 2005.

Pena Pitarch, E., Yang, J., and Abdel-Malek, K., (2005) “Santos^{TM} hand: A 25-Degree-of-Freedom Model,” *Proceedings of SAE Digital Human Modeling for Design and Engineering*, June 14-16, 2005, Iowa City, Iowa, USA.

Van der Helm, F.C. and Veenbaas, R. (1991), “Modelling the mechanical effect of muscles with large attachment sites: application to the shoulder mechanism,” *Journal of Biomechanics*, Vol. 24, No. 12, pp. 1151-1163.

Yang, J., Marler, R.T., Kim, H., Arora, J., and Abdel-Malek, K. (2004), “Multi-Objective Optimization for Upper Body Posture Prediction,” *10th AIAA/ISSMO Multidisciplinary Analysis and Optimization Conference,* Albany, New York, USA.

Yang, J., Marler, T., Kim, H.J., Farrell, K., Mathai, A., Beck, S., Abdel-Malek, K., Arora, J., and Nebel, K. (2005), “Santos^{TM}: A new Generation of Virtual Humans,” *SAE 2005 World Congress*, Cobo Center, Detroit, Michigan, USA.

Yang, J., Marler, T., Beck, S., Kim, J., Wang, Q., Zhou, X., Pena Pitarch, E., Farrell, K., Patrick, A., Potratz, J., Abdel-Malek, K., Arora, J., and Nebel, K. (2006a), “New Capabilities for the Virtual-Human Santos^{TM},” *SAE World Congress*, Cobo Center, Detroit, Michigan.

Yang, J., Marler R.T., Beck, S., Abdel-Malek, K, and Kim, J. (2006b). “Real-Time Optimal Reach Posture Prediction in a New Interactive Virtual Environment,” *Journal of Computer Science and Technology*, Vol. 21, No. 2, pp. 189-198.

CONTACT

Dr. Jingzhou Yang, Virtual Soldier Research (VSR) Program, Center for Computer-Aided Design, The University of Iowa, Iowa City, IA 52242, Tel: 319-353-2249, Fax: 319-384-0542, E-mail: jyang@engineering.uiowa.edu.